# Variational Monte Carlo study of a chiral spin liquid in the extended Heisenberg model on the kagome lattice

Wen-Jun Hu,[1] Wei Zhu,[1] Yi Zhang,[2] Shoushu Gong,[1] Federico Becca,[3] and D. N. Sheng[1]

[1]*Department of Physics and Astronomy, California State University, Northridge, California 91330, USA*
[2]*Department of Physics, Stanford University, Stanford, California 94305, USA*
[3]*Democritos National Simulation Center, Istituto Officina dei Materiali del CNR, and SISSA-International School
for Advanced Studies, Via Bonomea 265, I-34136 Trieste, Italy*

We investigate the extended Heisenberg model on the kagome lattice by using Gutzwiller projected fermionic states and the variational Monte Carlo technique. In particular, when both second- and third-neighbor superexchanges are considered, we find that a gapped spin liquid described by nontrivial magnetic fluxes and long-range chiral-chiral correlations is energetically favored compared to the gapless $U(1)$ Dirac state. Furthermore, the topological Chern number, obtained by integrating the Berry curvature, and the degeneracy of the ground state, by constructing linearly independent states, lead us to identify this flux state as the chiral spin liquid with a $C = 1/2$ fractionalized Chern number.

*Introduction.* Quantum spin liquids (QSLs) are exotic phases of strongly correlated spin systems which do not possess any local order even at zero temperature [1] but develop topological order due to the long-range entanglement in the system [2]. Various QSLs have been suggested as the ground state of some frustrated magnetic systems [1], and have been searched for many years in both experimental and theoretical studies. The kagome antiferromagnet is the most promising system for hosting QSLs [3–22]. In the corresponding Heisenberg model on the kagome lattice with nearest-neighbor interactions, a time-reversal symmetric QSL has been discovered by different advanced numerical methods, with gapped [16–19] or gapless excitations [13,14].

A subclass of QSLs, which breaks time-reversal symmetry, is called the chiral spin liquid (CSL) [23–26]. By doping the CSL, the condensation of the anyonic quasiparticles might realize exotic superconductivity [24,27,28]. The simplest CSL is given by the Kalmeyer-Laughlin state, which was proposed as the $\nu = 1/2$ fractional quantum Hall state in frustrated magnetic systems [23]. However, the realization of CSL by a spontaneous time-reversal symmetry breaking in realistic frustrated magnetic systems was elusive in the past [29,30]. Recently, the state-of-art density-matrix renormalization group (DMRG) has been implemented to study different spin-1/2 antiferromagnets on a kagome lattice with the spin couplings up to the third neighbors [20,21]. A CSL has been suggested as the $\nu = 1/2$ Laughlin state in these systems, based upon the calculation of the fractionally quantized Chern number $C = 1/2$ [20] and chiral edge spectrum [21]. Meanwhile, the same CSL has been also obtained in the Heisenberg model with explicit time-reversal symmetry breaking chiral interactions on the kagome lattice [22].

In theoretical studies, Wen *et al.* [24] described the CSL states through the fluxes of an underlying gauge field theory within the fermionic representation, which had shed light on the understanding of the topological order of the CSL, including the topological degeneracy and fractionalized quasiparticles [2,31–34]. Recently, Zhang *et al.* [35] revealed the semionic statistics of quasiparticles for the CSL state on a square lattice using the Gutzwiller projective fermionic

representation with the $\pi$-flux phase [24,36]. Motivated by the discovery of the CSL in extended kagome systems [20,21], recent variational studies based on the Gutzwiller projected parton wave function found that third-neighbor coupling could stabilize the CSL in the Heisenberg model on the kagome lattice [15]. This finding stimulates a deeper study and characterization (e.g., topological properties) of variational wave functions. In particular, it is interesting to compare the topological nature of such a CSL in the variational approach with the DMRG results [20,21,37].

In this Rapid Communication, we consider both the $J_1$-$J_2$-$J_3$ Heisenberg model,

$$H = J_1 \sum_{\langle ij \rangle} \vec{S}_i \cdot \vec{S}_j + J_2 \sum_{\langle\langle ij \rangle\rangle} \vec{S}_i \cdot \vec{S}_j + J_3 \sum_{\langle\langle\langle ij \rangle\rangle\rangle} \vec{S}_i \cdot \vec{S}_j, \quad (1)$$

and the $J_1$-$J_\chi$ model (with explicit chiral interactions),

$$H_\chi = J_1 \sum_{\langle ij \rangle} \vec{S}_i \cdot \vec{S}_j + J_\chi \sum_{\triangle/\triangledown} \vec{S}_i \cdot (\vec{S}_j \times \vec{S}_k), \quad (2)$$

on the kagome lattice. In the $J_1$-$J_2$-$J_3$ model, the system has first- ($J_1$), second- ($J_2$), and third-neighbor ($J_3$) couplings (the latter ones are only inside each hexagon), while in the $J_1$-$J_\chi$ model it has chiral couplings in each up ($\triangle$) and down ($\triangledown$) triangle, and the sites $i$, $j$, and $k$ follow the clockwise order in the triangles. In the following, we will take $J_1 = 1$ as the unit of energies.

Variational wave functions are constructed by projecting mean-field states in the fermionic representation. Through careful optimization of the variational parameters and simulations on large clusters, we compare the energies of the $U(1)$ Dirac spin liquid (DSL) and CSL. For the $J_1$-$J_2$-$J_3$ model, the CSL overcomes the DSL when $J_3$ is slightly larger than $J_2$. We would like to mention that, with even larger values of $J_3$, DMRG calculations suggested that the CSL has a transition to another spin ordered phase [37], but this issue is not addressed in the present Rapid Communication. For the $J_1$-$J_\chi$ model, a consistent energy gain is obtained for the CSL state at $J_\chi = 0.15$. The chiral-chiral correlation functions show a long-range chiral order, consistent with
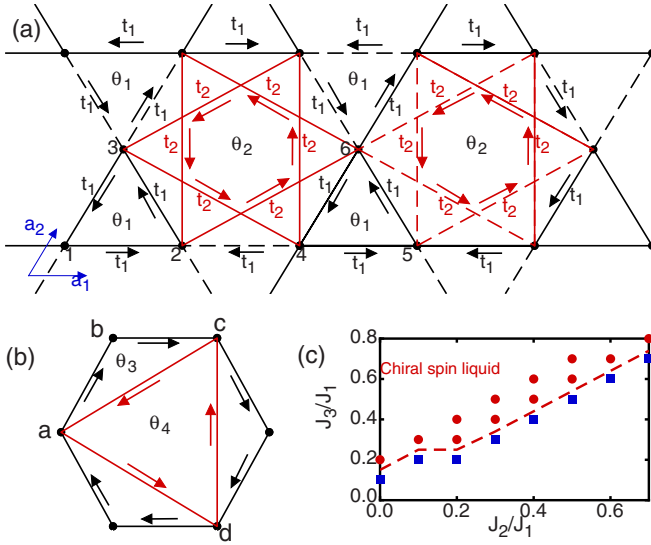
FIG. 1. (Color online) (a), (b) The variational ansatz with the NN hopping $t_1$ (black) and NNN hopping $t_2$ (red) is shown. Solid (dashed) lines indicate positive (negative) hoppings, which define the $U(1)$ DSL. The phases $\phi_1$ and $\phi_2$ are added upon this ansatz to obtain a CSL. The direction of the arrows indicates one possible convention of phases. In each up and down triangle, the flux is $\theta_1 = 3\phi_1$; in each hexagon, the flux is $\theta_2 = \pi - 6\phi_1$. The triangle $abc$ has flux $\theta_3 = \pi - 2\phi_1 - \phi_2$, and the triangle $acd$ has flux $\theta_4 = 3\phi_2$. (c) Phase diagram: The red dots (CSL) and blue squares [$U(1)$ DSL] are the calculated data. The red dashed line indicates the approximate phase boundary between the CSL and $U(1)$ DSL.

DMRG results. Most importantly, the calculation of the topological Chern number [26] allows us to conclude that the CSL in both models is equivalent to the $\nu = 1/2$ Laughlin state, as established in DMRG calculations [20,21]. Finally, we show that also the ground-state degeneracy, obtained by considering different boundary conditions in the mean-field Hamiltonian, is consistent with what expected from a CSL.

*Method and wave function.* The variational wave functions are defined by the projected mean-field states,

$$|\Psi_V\rangle = \mathcal{P}_G|\Psi_{\text{MF}}\rangle, \qquad (3)$$

where $\mathcal{P}_G = \prod_i (1 - n_{i\uparrow}n_{i\downarrow})$ is the Gutzwiller projector, which enforces no double occupation on each site. $|\Psi_{\text{MF}}\rangle$ is the ground state of a mean-field Hamiltonian that only contains hopping,

$$H_{\text{MF}} = \sum_{ij,\sigma} t_{ij}c_{i\sigma}^\dagger c_{j\sigma} + \text{H.c.}, \qquad (4)$$

where $c_{i,\sigma}^\dagger$ ($c_{i,\sigma}$) creates (destroys) an electron on site $i$ with spin $\sigma$. Different spin-liquid phases can be described by the different patterns of $t_{ij}$ on the bonds of the lattice. Here, we consider the hoppings for nearest-neighbor (NN) and next-nearest-neighbor (NNN) bonds, indicated by $t_1$ and $t_2$, respectively. Since we are interested in CSL, we allow for both real and imaginary parts in the hopping, i.e., $t_{ij} = |t_{ij}|e^{i\phi_{ij}}$. In Fig. 1, we show the ansatz of our variational wave function. Since $t_{ij}^* = t_{ji}$, an orientation of the bond is needed: For the

hopping from $i$ to $j$, $t_{ij}$ ($t_{ij}^*$) is taken in (opposite to) the direction of the arrow.

Here, we choose the case where the up and down triangles have the same fluxes (i.e., $\theta_1 = 3\phi_1$), and the flux in the hexagon is $\theta_2 = \pi - 6\phi_1$. This state can be represented as $[3\phi_1, \pi - 6\phi_1]$, as considered in Refs. [13,15]. When including also the NNN bonds, a more complex flux structure appears in the hexagon, as shown in Fig. 1: The triangles $abc$ have flux $\theta_3 = \pi - 2\phi_1 - \phi_2$, and the triangles $acd$ have flux $\theta_4 = 3\phi_2$. Thus, the variational state can be represented by using the four fluxes ($\theta_i$) as $[3\phi_1, \pi - 6\phi_1; \pi - 2\phi_1 - \phi_2, 3\phi_2]$. The $U(1)$ DSL, which has two Dirac points (for each spin), has fluxes $[0, \pi, \pi, 0]$, otherwise, the wave function describes a CSL [7]. In our calculations, we set the real part of the NN hopping $\text{Re}(t_1) = 1$, and tune the imaginary part $\text{Im}(t_1)$ to change $\phi_1$. For each $\phi_1$, we optimize the other two parameters [i.e., $\text{Re}(t_2)$ and $\text{Im}(t_2)$] using variational Monte Carlo to find the energetically favored state. In particular, we use the stochastic reconfiguration (SR) optimization method [38], which allows us to obtain an extremely accurate determination of variational parameters.

*Results.* We performed our variational calculations for the mean-field Hamiltonian Eq. (4) at half filling on toric clusters with $L \times L \times 3$ sites under the antiperiodic boundary conditions (APBCs), and compared the $U(1)$ DSL and the CSL. We start from the $U(1)$ DSL, and add the fluxes gradually through increasing $\phi_1$ to get the CSL. If we only consider the NN hopping term $t_1$ within the variational wave function, we find that, for $J_2 = J_3 > 0.3$, the CSL appears in the $J_1$-$J_2$-$J_3$ Heisenberg model as a local minimum. Most importantly, only when the NNN term $t_2$ is taken into account, the CSL has an energy gain with respect to the $U(1)$ DSL. Therefore, in the following, we use the wave function including both $\phi_1$ and $\phi_2$.

Our main results are presented in Fig. 2. For the $J_1$-$J_2$-$J_3$ Heisenberg model of Eq. (1), we find that the CSL is energetically favored when $J_3$ is a little larger than $J_2$. As an example in Fig. 2(a), we show that, at $J_2 = 0.5$ and $J_3 = 0.6$, the energy exhibits a minimum at a finite value of $\phi_1$, which is $\phi_1 = 0.0505\pi$ for $L = 8$ and $\phi_1 = 0.0567\pi$ for $L = 12$ and 16. It is quite time consuming to perform SR optimization on larger sizes, but, fortunately, the variational parameters are only slightly modified from $L = 12$ to $L = 16$ (see the Supplemental Material [39]). Therefore, we take the wave function optimized for $L = 16$ to calculate variational energies up to $L = 36$. After the finite-size scaling, which is shown in the inset of Fig. 2(a), the estimated energy per site at $J_2 = 0.5$ and $J_3 = 0.6$ is $E = -0.4387(1)$. In this case, the accuracy is about 5.8%, compared with the DMRG data on cylinder geometries (where $E = -0.465\,603$). By contrast, at $J_2 = J_3 = 0.5$ and up to $L = 12$, the best energy is given by the $U(1)$ DSL [see Fig. 2(b)]. However, when we take the optimized wave functions at each $\phi_1$ and perform the calculations up to $L = 28$, we find that the difference between the energies at $\phi_1 = 0$ and $0.0159\pi$ is very small (i.e., of the order of $10^{-4}$). Actually, performing the finite-size scaling yields the same estimated energy per site $E = -0.4420(1)$, as shown in the inset of Fig. 2(b). This point is very close to the boundary of the phase transition, thus it is hard to distinguish the CSL from the $U(1)$ DSL. More results for different values of $J_2$ and $J_3$ are shown in the Supplemental Material [39].
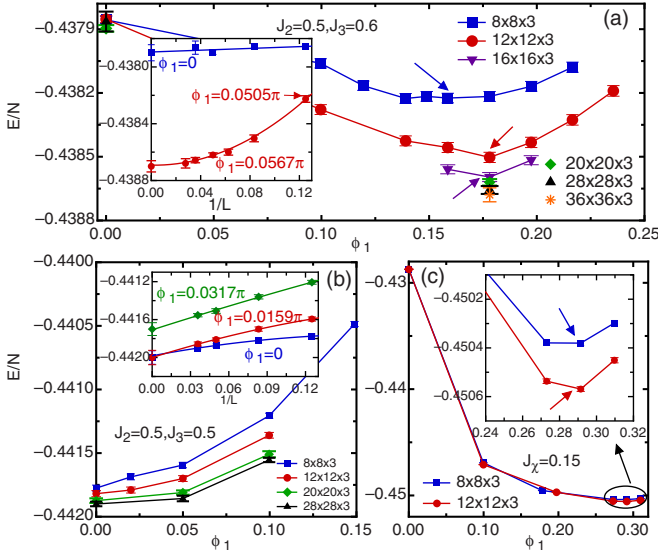
FIG. 2. (Color online) The energy per site as a function of $\phi_1$ on different lattices. Results for the $J_1$-$J_2$-$J_3$ Heisenberg model at $J_2 = 0.5$ with (a) $J_3 = 0.6$ and (b) 0.5, and (c) for the $J_1$-$J_\chi$ model at $J_\chi = 0.15$. Insets: The energy per site as function of $1/L$ for the $U(1)$ DSL ($\phi_1 = 0$) up to $L = 28$, and the CSL with $\phi_1 = 0.0505\pi$ on the $L = 8$ lattice and $\phi_1 = 0.0567\pi$ on larger clusters up to $L = 36$ (a); the finite-size effect for different $\phi_1$ (b) and with enlarged scale around $\phi_1 = 0.0928\pi$ (c). The arrows in (a) and (c) show the energy minimum, and indicate the CSL stabilized in both models.

The rough phase diagram for the $J_1$-$J_2$-$J_3$ Heisenberg model is presented in Fig. 1(c). Here, for $J_2 = 0$, we get the CSL for $J_3 \geqslant 0.2$, which is different from the conclusion in Ref. [15], which obtained $J_3 > 0.3$. The reason for this discrepancy might be due to the energy gain obtained by including the NNN hopping $t_2$ in the variational wave function.

In order to detect the chiral order in the optimized wave functions, we measure the chiral-chiral correlation function between two triangles defined as

$$\langle \chi_i \chi_j \rangle = \left\langle \left[ \vec{S}_1^i \cdot \left( \vec{S}_2^i \times \vec{S}_3^i \right) \right] \left[ \vec{S}_1^j \cdot \left( \vec{S}_2^j \times \vec{S}_3^j \right) \right] \right\rangle, \quad (5)$$

where $\chi_i = \vec{S}_1^i \cdot (\vec{S}_2^i \times \vec{S}_3^i)$ is the chirality of triangle $\triangle_{123}^i$. In Fig. 3, we show the chiral-chiral correlation $\langle \chi_i \chi_j \rangle$ as a function of the distance $|i - j|$ between two up triangles at $J_2 = 0.5$ and $J_3 = 0.6$ on $8 \times 8 \times 3$ and $12 \times 12 \times 3$ lattices. On both clusters, $\langle \chi_i \chi_j \rangle$ decays rapidly to a finite value, indicating the long-range chiral order, the difference between $L = 8$ and 12 being small. It is interesting to note that the chiral order is larger in the accurate DMRG calculations (performed on a cylinder with $L = 6$) than in variational Monte Carlo ones.

The variational state with nontrivial fluxes ($[3\phi_1, \pi - 6\phi_1; \pi - 2\phi_1 - \phi_2, 3\phi_2]$) can be also implemented to the $J_1$-$J_\chi$ model of Eq. (2). In this case, the CSL is stabilized much easier: Even for a small value of $J_\chi$, namely, $J_\chi = 0.15$, there is a clear minimum in the energy around $\phi_1 = 0.0928\pi$ [see Fig. 2(c)]. For $L = 12$, the CSL has an energy per site $E = -0.450\,57(1)$, much lower than $E = -0.428\,72(2)$ of the $U(1)$ DSL. Also the chiral-chiral correlation function in Fig. 3 indicates a robust chiral order at $J_\chi = 0.15$.
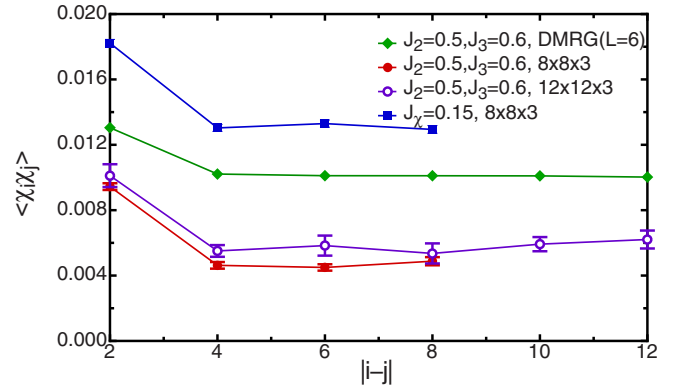


FIG. 3. (Color online) The chiral-chiral correlation function along the $\vec{a}_1$ direction on $L = 8$ and 12 lattices for the $J_1$-$J_2$-$J_3$ Heisenberg model (at $J_2 = 0.5$ and $J_3 = 0.6$) and the $J_1$-$J_\chi$ model (at $J_\chi = 0.15$). The DMRG data are calculated on a cylinder with $L = 6$ at $J_2 = 0.5$ and $J_3 = 0.6$.

Until now, we have shown that the chiral state arises in these two models in view of the chiral-chiral correlation. However, a CSL is further characterized by the nontrivial topological structures, including the topological Chern number [26] and the degeneracy of the ground state [2]. In the following, we proceed in these two directions to clarify that our variational state indeed represents a CSL state.

First, the topological Chern number is computed as the integral over the Berry curvature $F(\Theta_1, \Theta_2)$ [40–43],

$$C = \frac{1}{2\pi} \int d\Theta_1 d\Theta_2 F(\Theta_1, \Theta_2), \quad (6)$$

where $0 \leqslant \Theta_k \leqslant 2\pi$ ($k = 1, 2$). To compute the Chern number numerically, we consider twisted boundary conditions in the mean-field Hamiltonian, namely, $c_{j+L_k \uparrow} = c_{j\uparrow} e^{i\Theta_k}$ and $c_{j+L_k \downarrow} = c_{j\downarrow} e^{-i\Theta_k}$. Then, we divide the the Brillouin zone into $M$ plaquettes, with the Berry curvature being $F_l = \arg \prod_i \langle \Psi_V^{l_{i+1}} | \Psi_V^{l_i} \rangle$ ($l = 1, \ldots, M$; $i = 1, 2, 3, 4$ for the four corners of the $l$th plaquette, and $\Psi_V^{l_5} = \Psi_V^{l_1}$), where $|\Psi_V^l\rangle$ is the projected ground state of the mean-field Hamiltonian with twisted boundary conditions. The overlap $\langle \Psi_V^{l_{i+1}} | \Psi_V^{l_i} \rangle = \sum_x P(x) \frac{\langle x | \Psi_V^{l_i} \rangle}{\langle x | \Psi_V^{l_{i+1}} \rangle}$ is calculated by the Monte Carlo method according to the weight $P(x) = \frac{|\langle x | \Psi_V^{l_{i+1}} \rangle|^2}{\sum_x |\langle x | \Psi_V^{l_{i+1}} \rangle|^2}$. In order to numerically check the accuracy, we changed $M$ from 100 up to 400 plaquettes. The numerical results show that the dimension of mesh changes the Berry curvature, but gives the same topological Chern number. We must emphasize that the integration from 0 to $2\pi$ in the twist of the fermionic operators includes two periods of phases for the spin operators and, therefore, the result must be divided by 4. The integration between 0 and $2\pi$ gives 2 with high accuracy (see Fig. 4), leading to $C = 1/2$, which is fully consistent with recent DMRG results [20].

The degeneracy of the wave function, which indicates a nontrivial ground-state structure, was not obvious to obtain from the variational approach with the Gutzwiller projected parton construction. Recently, Zhang *et al.* [35] realized that the ground-state degeneracy is consistent with the linear
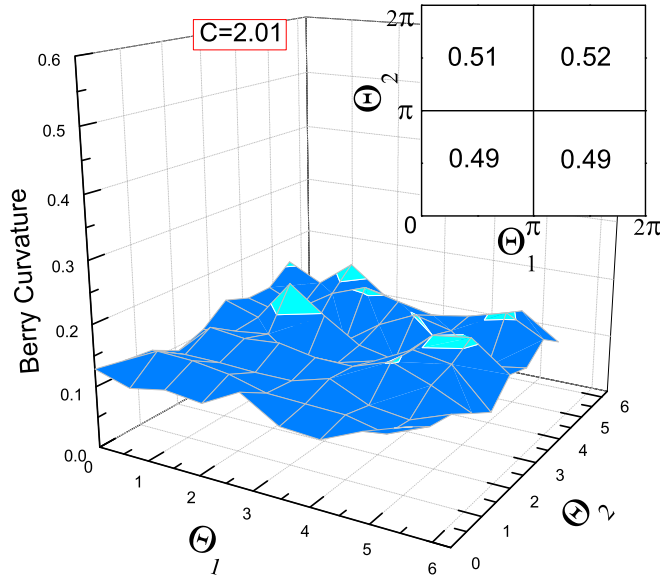
FIG. 4. (Color online) The Berry curvature at $J_2 = 0.5$ and $J_3 = 0.6$ on a $L = 12$ lattice. The Brillouin zone is divided into a mesh with 100 plaquettes. The summation between 0 and $2\pi$ gives $C = 2.01$.

dependence for variational wave functions through fermionic construction for SU(2) Chern-Simons theory. We follow the same idea to construct the linearly independent states from the four projected states that are obtained through changing the boundary conditions of the mean-field Hamiltonian in the $\vec{a}_1$ and $\vec{a}_2$ directions (see Fig. 1). We denote the four states as $|\psi_1, \psi_2\rangle$, where $\psi_i = 0$ for the periodic boundary condition and $\pi$ for the antiperiodic boundary condition ($i = 1, 2$). In order to find the linearly independent states from these four projected states (i.e., $\{|0,0\rangle, |0,\pi\rangle, |\pi,0\rangle, |\pi,\pi\rangle\}$), we calculate the overlaps between all possible states. The numerical calculations up to $L = 32$ indicate strong size effects, due to the smallness of the mean-field gap. For example, for $J_2 = 0.5$ and $J_3 = 0.6$ on the $16 \times 16 \times 3$ lattice with $\phi_1 = 0.0567\pi$ and $\phi_2 = -0.2807\pi$, the band gap is only about 0.6.

Thus, in order to suppress the finite-size effects on small clusters, we tune $\phi_1$ and $\phi_2$ to enlarge the mean-field band

gap (up to a value of 2), still keeping the long-range chiral order and a nonzero Chern number. Consequently, even on the small $8 \times 8 \times 3$ lattice, we find the two linear independent states indicating the twofold degeneracy, which are (see the Supplemental Material [39] for details)

$$|1\rangle = |00\rangle = \frac{1}{\sqrt{3}}(|0,\pi\rangle + |\pi,0\rangle + |\pi,\pi\rangle), \qquad (7)$$

$$|2\rangle = \frac{1}{\sqrt{6}}(|0,\pi\rangle + e^{i\frac{2\pi}{3}}|\pi,0\rangle + e^{-i\frac{2\pi}{3}}|\pi,\pi\rangle). \qquad (8)$$

*Conclusions.* In conclusion, we investigated the CSL in the $J_1$-$J_2$-$J_3$ Heisenberg models on the kagome lattice by the variational approach with Gutzwiller projected fermionic construction. Our variational studies reveal that the CSL is energetically favored in the phase region consistent with recent DMRG calculations [20]. However, differently from the DMRG results, we found that when $J_3$ is larger than $J_2$, instead of $J_2 = J_3$, the CSL begins to appear as indicated by the existence of an energy minimum while tuning the fluxes. On the other hand, we have shown that our wave function also works for the $J_1$-$J_\chi$ model, which includes a three-spin-parity and time-reversal violating interaction.

Further investigations with these optimized wave functions show that the spin-spin correlation functions decay fast (see the Supplemental Material [39]), indicating short-range correlations. Instead, the chiral-chiral correlation function presents a long-range chiral order, consistent with DMRG results. The variational wave function underestimates the robustness of the CSL, as the accurate DMRG calculations show stronger chiral order than a variational state. Moreover, our calculations of the topological Chern number and the ground-state degeneracy suggest that the chiral state is the $\nu = 1/2$ Laughlin state.

[1] L. Balents, Nature (London) **464**, 199 (2010).

[2] X.-G. Wen, Phys. Rev. B **40**, 7387 (1989); Int. J. Mod. Phys. B **4**, 239 (1990); X.-G. Wen and Q. Niu, Phys. Rev. B **41**, 9377 (1990).

[3] P. A. Lee, Science **321**, 1306 (2008).

[4] P. Mendels and F. Bert, J. Phys.: Conf. Ser. **320**, 012004 (2011).

[5] T.-H. Han, J. S. Helton, S. Chu, D. G. Nocera, J. A. Rodriguez-Rivera, C. Broholm, and Y. S. Lee, Nature (London) **492**, 406 (2012).

[6] J. Marston and C. Zeng, J. Appl. Phys. **69**, 5962 (1991).

[7] M. B. Hastings, Phys. Rev. B **63**, 014413 (2000).

[8] L. Balents, M. P. A. Fisher, and S. M. Girvin, Phys. Rev. B **65**, 224412 (2002).

[9] F. Wang and A. Vishwanath, Phys. Rev. B **74**, 174423 (2006).

[10] M. Hermele, Y. Ran, P. A. Lee, and X.-G. Wen, Phys. Rev. B **77**, 224413 (2008).

[11] Y.-M. Lu, Y. Ran, and P. A. Lee, Phys. Rev. B **83**, 224413 (2011); Y.-M. Lu, G. Y. Cho, and A. Vishwanath, arXiv:1403.0575.

[12] L. Messio, B. Bernu, and C. Lhuillier, Phys. Rev. Lett. **108**, 207204 (2012).

[13] Y. Ran, M. Hermele, P. A. Lee, and X.-G. Wen, Phys. Rev. Lett. **98**, 117205 (2007).

[14] Y. Iqbal, F. Becca, and D. Poilblanc, Phys. Rev. B **84**, 020407 (2011); Y. Iqbal, F. Becca, S. Sorella, and D. Poilblanc, *ibid.* **87**, 060405 (2013); Y. Iqbal, D. Poilblanc, and F. Becca, *ibid.* **89**, 020407 (2014).

[15] J.-W. Mei and X.-G. Wen, arXiv:1407.0869.

[16] H. C. Jiang, Z. Y. Weng, and D. N. Sheng, Phys. Rev. Lett. **101**, 117203 (2008).

[17] S. Yan, D. Huse, and S. White, Science **332**, 1173 (2011).

[18] S. Depenbrock, I. P. McCulloch, and U. Schollwöck, Phys. Rev. Lett. **109**, 067201 (2012).

[19] H. C. Jiang, Z. Wang, and L. Balents, Nat. Phys. **8**, 902 (2012).

[20] S. S. Gong, W. Zhu, and D. N. Sheng, Sci. Rep. **4**, 6317 (2014).

[21] Y. C. He, D. N. Sheng, and Y. Chen, Phys. Rev. Lett. **112**, 137202 (2014).

[22] B. Bauer, B. P. Keller, M. Dolfi, S. Trebst, and A. W. W. Ludwig, arXiv:1303.6963; B. Bauer, L. Cincio, B. P. Keller, M. Dolfi, G. Vidal, S. Trebst, and A. W. W. Ludwig, Nat. Commun. **5**, 5137 (2014).

[23] V. Kalmeyer and R. B. Laughlin, Phys. Rev. B **39**, 11879 (1989).

[24] X.-G. Wen, F. Wilczek, and A. Zee, Phys. Rev. B **39**, 11413 (1989).

[25] K. Yang, L. K. Warman, and S. M. Girvin, Phys. Rev. Lett. **70**, 2641 (1993).

[26] F. D. M. Haldane and D. P. Arovas, Phys. Rev. B **52**, 4223 (1995).

[27] R. B. Laughlin, Phys. Rev. Lett. **60**, 2677 (1988).

[28] F. Wilczek, *Fractional Statistics and Anyon Superconductivity* (World Science, Singapore, 1990).

[29] D. F. Schroeter, E. Kapit, R. Thomale, and M. Grelter, Phys. Rev. Lett. **99**, 097202 (2007).

[30] A. E. B. Nielsen, J. I. Cirac, and G. Sierra, Phys. Rev. Lett. **108**, 257206 (2012).

[31] F. Wilczek and A. Zee, Phys. Rev. Lett. **52**, 2111 (1984).

[32] R. B. Laughlin, Phys. Rev. Lett. **50**, 1395 (1983).

[33] D. Arovas, J. R. Schrieffer, and F. Wilczek, Phys. Rev. Lett. **53**, 722 (1984).

[34] X.-G. Wen, Phys. Rev. B **44**, 2664 (1991).

[35] Y. Zhang, T. Grover, and A. Vishwanath, Phys. Rev. B **84**, 075128 (2011); Y. Zhang, T. Grover, A. Turner, M. Oshikawa, and A. Vishwanath, *ibid.* **85**, 235151 (2012); Y. Zhang and A. Vishwanath, *ibid.* **87**, 161113 (2013).

[36] A. W. W. Ludwig, M. P. A. Fisher, R. Shankar, and G. Grinstein, Phys. Rev. B **50**, 7526 (1994).

[37] S. S. Gong, W. Zhu, L. Balents, and D. N. Sheng arXiv:1412.1571.

[38] S. Sorella, Phys. Rev. B **71**, 241103 (2005).

[39] See Supplemental Material at http://link.aps.org/supplemental/10.1103/PhysRevB.91.041124 for more numerical data and the derivation of the two linearly independent states.

[40] Q. Niu, D. J. Thouless, and Y.-S. Wu, Phys. Rev. B **31**, 3372 (1985).

[41] D. N. Sheng, Xin Wan, E. H. Rezayi, Kun Yang, R. N. Bhatt, and F. D. M. Haldane, Phys. Rev. Lett. **90**, 256802 (2003).

[42] X. Wan, D. N. Sheng, E. H. Rezayi, Kun Yang, R. N. Bhatt, and F. D. M. Haldane, Phys. Rev. B **72**, 075325 (2005).

[43] M. Hafezi, A. S. Sørensen, M. D. Lukin, and E. Demler, Europhys. Lett. **81**, 10005 (2008).